HHS Public Access

Author manuscript

*J Cell Biochem*. Author manuscript; available in PMC 2018 August 01.

Published in final edited form as:

*J Cell Biochem*. 2017 August ; 118(8): 2231–2240. doi:10.1002/jcb.25874.

# Lnk Deficiency leads to TPO-Mediated Osteoclastogenesis and Increased Bone Mass Phenotype

**David J. Olivos III**[1,2,*], **Marta Alvarez**[1,*], **Ying-Hua Cheng**[1], **R. Adam Hooker**[1], **Wendy A. Ciovacco**[1,5], **Monique Bethel**[1], **Haley McGough**[1], **Christopher Yim**[1], **Brahmananda R. Chitteti**[3], **Pierre P. Eleniste**[4], **Mark C. Horowitz**[5], **Edward F. Srour**[2,3,7], **Angela Bruzzaniti**[4], **Robyn K. Fuchs**[6], and **Melissa A. Kacena**[1,5]

[1]Department of Orthopaedic Surgery, Indiana University School of Medicine, Indianapolis, Indiana

[2]Department of Microbiology and Immunology, Indiana University School of Medicine, Indianapolis, Indiana

[3]Department of Medicine, Indiana University School of Medicine, Indianapolis, Indiana

[4]Department of Biomedical and Applied Sciences, Indiana University School of Dentistry, Indianapolis, Indiana

[5]Department of Orthopaedics and Rehabilitation, Yale University School of Medicine, New Haven, Connecticut

[6]Department of Physical Therapy, Indiana University School of Health and Rehabilitation Sciences, Indianapolis, Indiana

[7]Department of Pediatrics, Indiana University School of Medicine, Indianapolis, Indiana

## Abstract

The Lnk adapter protein negatively regulates the signaling of thrombopoietin (TPO), the main megakaryocyte (MK) growth factor. Lnk-deficient (−/−) mice have increased TPO signaling and increased MK number. Interestingly, several mouse models exist in which increased MK number leads to a high bone mass phenotype. Here we report the bone phenotype of these mice. MicroCT and static histomorphometric analyses at 20 weeks showed the distal femur of $Lnk^{-/-}$ mice to have significantly higher bone volume fraction and trabecular number compared to wild-type (WT) mice. Notably, despite a significant increase in the number of osteoclasts (OCs), and decreased bone formation rate in $Lnk^{-/-}$ mice compared to WT mice, $Lnk^{-/-}$ mice demonstrated a 2.5-fold greater BV/TV suggesting impaired OC function *in vivo*. Additionally, $Lnk^{-/-}$ mouse femurs exhibited non-significant increases in mid-shaft cross-sectional area, yet increased periosteal BFR compared to WT femurs was observed. $Lnk^{-/-}$ femurs also had non-significant increases in polar moment of inertia and decreased cortical bone area and thickness, resulting in reduced bone stiffness, modulus, and strength compared to WT femurs. Of note, Lnk is expressed by OC lineage cells and when $Lnk^{-/-}$ OC progenitors are cultured in the presence of TPO, significantly more

Corresponding Author: Melissa A. Kacena, Ph.D., August M. Watanabe Translational Scholar, Showalter Scholar, Associate Professor of Orthopaedic Surgery, Indiana University School of Medicine, 1130 West Michigan Street, FH 115, Indianapolis, IN 46202, (317) 278-3482 – phone, (317) 278-9568 – fax, mkacena@iupui.edu.

*Contributed equally to this work

OCs are observed than in WT cultures. Lnk is also expressed in osteoblast (OB) cells and in vitro reduced alkaline phosphatase activity was observed in $Lnk^{-/-}$ cultures. These data suggest that both direct effects on OB and OC as well as indirect effects of MKs in regulating OB contributes to the observed high bone mass.

**Keywords**

Lnk; Osteoclasts; Megakaryocytes; Osteoblasts; Bone Mass; Bone Phenotype

## INTRODUCTION

The Lnk adaptor protein (SH2B3) is expressed in hematopoietic tissue and is a known negative regulator of cytokine and growth factor signaling in hematopoiesis and lymphopoiesis [Huang et al., 1995; Takaki et al., 1997]. $Lnk^{-/-}$ genetically engineered mouse models have been instrumental in elucidating the physiologic function of Lnk. Takaki et al [Takaki et al., 2000] showed that $Lnk^{-/-}$ mice experience defective B lymphocyte production resulting in elevated numbers of B cells in bone marrow (BM), and accumulation of B cell progenitors in the spleen. In $Lnk^{-/-}$ mice, Velazquez et al [Velazquez et al., 2002] also observed increased extramedullary production of MK and erythrocytes resulting in splenomegaly, and increased MK and B cells in the BM and lymph nodes, respectively. Peripheral blood analysis revealed significant increases in circulating leukocytes and platelets. Partly due to $Lnk^{-/-}$ cell hypersensitivity to cytokines, *In vitro* analysis demonstrated a significant increase in hematopoietic progenitor proliferation and absolute number [Velazquez et al., 2002].

Additionally, Lnk is highly expressed in erythroid, MK, and myeloid lineage stem cells. These findings suggest Lnk functions as a negative modulator of hematopoietic cell proliferation. Furthermore, by exploring Lnk and TPO interactions, Tong and Lodish [Tong and Lodish, 2004] found Lnk to negatively regulate TPO induced hematopoietic cell proliferation through TPO-c-mpl inhibition. Accordingly, $Lnk^{-/-}$ mice would be predicted to exhibit elevated TPO-c-mpl signaling and consequently increased TPO-c-mpl mediated cell proliferation. $Lnk^{-/-}$ mice displayed increased numbers of MK and ploidy in the BM and spleen. Consistent with these findings, $Lnk^{-/-}$ MK exhibited enhanced *in vitro* proliferative response through STAT3, STAT5, Akt and MAPK signaling pathways. Hence, Lnk has been well established as a key mediator of hematopoiesis and role player in MK proliferation and development.

MK are hematopoietic thrombocyte progenitor cells that originate in the BM. Burgeoning research demonstrates MK to play a critical role in skeletal homeostasis by surrounding and interconnecting functionally with bone cells [Kacena et al., 2006a; Kacena et al., 2006b]. *In vitro* studies confirm MK express and/or secrete several bone-related proteins that stimulate OB proliferation and bone formation [Beeton et al., 2006; Bord et al., 2005; Breton-Gorius et al., 1992; Chagraoui et al., 2003; Cheng et al., 2013; Cheng et al., 2015; Chenu and Delmas, 1992; Ciovacco et al., 2010; Ciovacco et al., 2009; Eleniste et al., 2016; Frank et al., 1993; Kacena et al., 2012; Kacena et al., 2006b; Kelm et al., 1992; Pearse et al., 2001;

Sipe et al., 2004; Thiede et al., 1994]. Furthermore, at least 4 mouse models have been described in which significantly elevated MK numbers lead to increases in bone mass. TPO overexpression in mice leads to approximately a 4-fold increase in MK number and an osteosclerotic bone phenotype [Villeval et al., 1997; Yan et al., 1996]. We previously demonstrated that mice deficient in GATA-1 or NF-E2, transcription factors required for mature MK development, had elevated numbers of MK and developed high bone mass [Kacena et al., 2005; Kacena et al., 2004]. More recently, a similar phenotype exhibiting increased MK numbers accompanied by high bone mass phenotype was observed in a platelet-type von Willebrand disease mouse model with a gain-of-function (GOF) mutation [Suva et al., 2008]. In the current study, we examine whether $Lnk^{-/-}$ deficiency in mice regulates bone mass phenotype.

## METHODS

### MICE

For these studies 5-month-old female and male WT C57BL/6 and $Lnk^{-/-}$ mice were utilized. $Lnk^{-/-}$ mice are on a C57BL/6 background and were kindly provided by Dr. T. Pawson (Samuel Lunenfeld Research Institute, Toronto, Canada), and C57BL/6 mice were obtained from Jackson Laboratories (Maine). The generation and breeding of $Lnk^{-/-}$ mice was previously described [Tong and Lodish, 2004; Velazquez et al., 2002]. The Institutional Animal Care and Use Committee (IACUC) of the Indiana University School of Medicine approved all procedures. NIH Guidelines and the Guide for the Care and Use of Laboratory Animals were followed.

### HISTOMORPHOMETRY

Actively forming bone surfaces of WT and $Lnk^{-/-}$ mice were labeled by intraperitoneal (IP) injections of the fluorochrome calcein (30mg/kg; Sigma) at 13 and 3 days prior to sacrifice. At sacrifice, the left femur was removed and stored in 10% neutral buffered formalin for 24-hours, followed by storage in 70% alcohol. The right femur was removed, wrapped in saline soaked gauze and stored at −80C for biomechanical analysis. Femoral trabecular (distal region) and cortical (mid-shaft region) bone was analyzed by static and dynamic histomorphometry as previously described [Feher et al., 2010; Warden et al., 2008]. Mid-sagittal sections of 8 μm were cut by a Reichert-Jung 2050 microtome (Magee Scientific, Inc) and stained with McNeal's tetrachrome for static histomorphometry. Mid-sagittal sections of 8 μm were cut and left unstained for dynamic histomorphometry and wall thickness analysis. A semiautomatic analysis system (Bioquant OSTEO 7.20.10, Bioquant Image Analysis Co.) attached to a microscope with an ultraviolet light source (Nikon Optiphot 2 microscope, Nikon) was used to make histological measurements on one stained (static) and unstained (dynamic) section for each animal.

### Micro-Computed Tomogograhy

As previously described, micro-computed tomography (microCT; Skyscan 1172; Skyscan, Kontich, Belgium) was used to quantify trabecular and cortical bone parameters of the distal and mid-shaft femur [Feher et al., 2010; Warden et al., 2008; Weatherholt et al., 2013]. Femurs were scanned at with at an energy level of 60 Kv, isotropic voxel size of 9μm, and

0.5mm filter, while a 1mm thick region of trabecular bone was analyzed at 0.5 mm distal to the growth plate. Binarized images were used to calculate the following three-dimensional bone volume parameters: trabecular bone volume (BV/TV, %), trabecular number (Tb.N, 1/mm), trabecular thickness (Tb.Th, mm), and trabecular separation (Tb.Sp, mm) using NRecon reconstruction software (Skyscan).

## BIOMECHANICS

A materials testing device (MTS Systems Corporation; Eden Prairie, MN) was used to determine relative bone strength by three-point bending as previously described [Feher et al., 2010; Warden et al., 2008; Weatherholt et al., 2013]. The right femurs were thawed to room temperature in a saline bath for 2h prior to testing. Femurs were placed in a saline bath at 37°C and stabilized with a static preload of 1 N in the anterior-posterior direction, and loaded to failure with a crosshead speed of 10 mm/min. Calculations of force (N), stiffness (N/mm), polar moment of inertia, ultimate stress (MPa), modulus (MPa), and toughness ($MJ/m^3$) were computed from force versus displacement data collected at 100 Hz.

## PREPARATION OF NEONATAL CALVARIAL CELLS (OB)

Neonatal murine calvarial OB were prepared from WT C57BL/6 and $Lnk^{-/-}$ mice as previously described [Chitteti et al., 2010]. Our technique was modified from the basic method described by Wong and Cohn [Wong and Cohn, 1975]. Dissected neonatal mice calvarias were treated with EDTA in PBS for 30 min and subjected to sequential collagenase digestions (200 U/ml). The starting OB population consisting of ~90% OB and OB precursors were collected from fractions 3–5 where digestions were incubated at 37°C for 20–35, 35–50, and 50–65 min, respectfully [Horowitz et al., 1994; Jilka and Cohn, 1981; Simmons et al., 1982]. Seeded at optimal pre-tested conditions ($2x10^4$ cells/ml), OB were maintained in αMEM supplemented with 10% fetal bovine serum (FBS), ascorbic acid (50 μg/ml added on day 0, and at all feedings), and β-glycerophosphate (5mM added starting on day 7, and all subsequent feedings). Cells were replenished twice per week, and some cultures were administered TPO (100 ng/ml) to stimulate MK as described [Meijome et al., 2015].

## PREPARATION OF FETAL LIVER DERIVED MEGAKARYOCYTES

Murine MK were prepared as previously described [Kacena et al., 2006b; Kacena et al., 2004]. Fetal livers obtained from pregnant C57BL/6 mice at E13–15 were prepared into single cell suspensions, washed, and cultured in 100 ml dishes with Dulbecco modified eagle medium (DMEM) supplemented with 10% fetal calf serum (FCS) and 1% murine TPO [Villeval et al., 1997]. A 90–95% pure MK population was isolated from lymphocytes and other cell types using a one-step albumin gradient after ~5 days [Drachman et al., 1997].

## CELL CYCLE ANALYSIS

A FACS caliber flow cytometer (BDIS) was used to determine the percentage of cells in G0/G1 and S/G2 + M phases of WT C57BL/6 and $Lnk^{-/-}$ calvarial OB on days 1, 3, 5, and 7 of culture. Cells were prepared as previously described [Srour et al., 1992]. OB were

labeled with a staining cocktail mixture of propidium iodide (0.1 mg/ml), Nonidet P40 (0.6%) in PBS (1:1; v/v), and RNase (2 mg/ml) prior to mixing and 30 min ice incubation.

## APOPTOSIS ANALYSIS

A FACs caliber flow cytometer (BDIS) was used to assess apoptosis of WT C57BL/6 and $Lnk^{-/-}$ calvarial OB on days 1, 3, 5, and 7 of culture. Cells were washed once in DMEM, incubated on ice for 15 min, and stained with the highly fluorescent allophycocyanin (APC) annexin V conjugate (eBioscience, San Diego, CA). Cells were washed and re-suspended with DMEM, stained with 10 μl of 10 ng/ml propidium iodide, and incubated at RT before analysis.

## ALKALINE PHOSPHATASE ACTIVITY

The colorimetric conversion hydrolyzing *p*-nitrophenol phosphate to *p*-nitrophenol (Sigma, St. Louis, MO) was used to determine alkaline phosphatase activity. Samples were normalized to total protein BCA (Pierce, Waltham, MA) [Hughes and Aubin, 1998]. Calvarial OB at 2 days old were cultured for 14 days, washed with PBS (2X) and lysed with 0.1% (v/v) Triton X-100 containing protease inhibitors (Pierce, Waltham, MA). Lysates were then subjected to two freeze-thaw cycles, centrifuged, and incubated with 3 mg/ml *p*-nitrophenol phosphate in an alkaline buffer, pH 8.0, (Sigma, St. Louis, MO) for 30 min at 37°C. NaOH (20 mM) conversion of *p*-nitrophenol to p-nitrophenolate quenched the enzyme-catalyzed reaction. Plates were read at 395 nM (GENios Plus, Tecan) and alkaline phosphate enzyme activity was determined by comparison with known *p*-nitrophenol standards (Sigma, St. Louis, MO).

## QUANTITIVE ANALYSIS OF CALCIUM DEPOSITION

Neonatal calvarial OB were analyzed for calcium deposition after 2 weeks of culture by eluting Alizarin Red S (Sigma Chemical Co., St. Louis, MO) from OB monolayers as previously described [Stanford et al., 1995]. Cell monolayers were washed with PBS (2X), fixed in ice-cold ethanol (70%; v/v) for 1 h, and washed with water (2X). Alizarin Red S (40mM; pH 4.2) staining was achieved after 10 min shaking at RT, then unbound dye was removed by washing with water (5X) and with PBS (1X for 15min, RT, shaking). To elute bound Alizarin Red for quantification, OB monolayers were incubated for 15 min at RT under shaking with cetypyridinium chloride (1%; v/v) in sodium-phosphate (10mM; pH 7.0). Absorbance from aliquots was measured at 562 nm (GENios Plus, Texan), and Alizarin Red concentrations were calculated from measured standards (Ca/mol of dye in solution).

## PREPARATION OF BONE MARROW CELLS

WT C57BL/6 and $Lnk^{-/-}$ mice tibiae and femurs were dissected at 6–10 weeks of age. Following removal of the epiphyses, the BM was flushed with a 27-gauge needle and syringe using 2–3 mls of ice cold α-MEM supplemented with 10% FCS (v/v).

BM cells were suspended into single cells and washed twice prior to use.

## PREPARATION OF BONE MARROW MACROPHAGES

BM cells were prepared as above. BM cells at $5x10^7$ cells/ml were cultured in 100 mm tissue culture dishes containing α-MEM supplemented with 10% FCS and 20 ng/ml of M-CSF (Peprotech, Rocky Hill, NJ). After 3 days in culture, adherent cells were dislodged with trypsin, and adjusted to 1 x $10^5$ cells/ml concentration for OC generation as described below.

## IN VITRO OSTEOCLAST-LIKE CELL FORMATION MODELS

BMM ($1x10^5$) were cultured in α-MEM supplemented with 10% FCS, 30 ng/ml of M-CSF (R&D Systems, Minneapolis, MN), and 50 ng/ml RANKL (R&D Systems, Minneaspolis, MN). Media was changed every third day for 6–8 days pending OC formation, fixed with 2.5% glutaraldehyde in PBS for 30 minutes at RT, and TRAP stained. Only $TRAP^+$ multinucleated cells (>3 nuclei) were quantified. TPO (100 ng/ml; Peprotech, Rocky Hill, NJ) was added to some cultures.

## CELL STIMULATION AND LYSIS

BMM, RAW 264.7, MK, and Ba/F3 cells from C57BL/6 and $Lnk^{-/-}$ or cell lines grown to ~75% confluency were treated with reduced serum media (0.5%) for 16–18 hours. Cells were treated with human recombinant TPO (100 ng/ml) for 0, 1, 3, 5, 10, and 30 min in the presence of 100 μM sodium orthovanadate. Immediately after each incubation period, cells were rinsed twice with inhibitor-laced ice-cold (Halt Protease Inhibitor Cocktail and Halt Phosphatase Cocktail, Pierce). After aspirating the PBS and inhibitor wash, cells were placed (adherent cells were scraped) in lysis buffer containing: Tris (20 mM; pH7.2), NaCl (150 mM), Triton X-100 (1.0%), sodium deoxycholate (1.0%), SDS (0.1%), EDTA (5.0 mM), and protease and phosphatase inhibitors (Pierce). Lysates were centrifuged at 12,000 x g for 15 min at 4°C, and supernatants were collected. Protein concentration was determined using a BCA protein assay kit with BSA as the standard. Each sample was normalized for protein concentration prior to immunoprecipitation (IP) analyses or Western blotting.

## IMMUNOPRECIPITATION ASSAYS AND WESTERN BLOTTING

For IP analyses, OB were rinsed with ice-cold PBS and lysed in modified RIPA (mRIPA) buffer containing Tris-HCl (50 mM; pH 7.4), NaCl (150mM), EDTA (5mM), NP40 (1%), sodium deoxycholate (1%), SDS (0.1%), NaF (50mM), aprotinin (1%), and $Na_3VO_4$ (0.1 mM). To obtain soluble cell extracts, cells were further lysed by sonication and centrifuged at 13,000 rpm for 5 min at 4°C. Approximately 150 μg of lysates were incubated with 3 μg of Lnk antibody from Millipore (Billerica, MA) for 2h at 4°C. After incubation, 20 μl of Protein G-agarose beads were added to individual tubes for 1h at 4°C. Beads were washed four times with mRIPA before washing once with 40 μl of 2X Laemmli's sample buffer with β-mercaptoethanol, and immunoblotted with an anti-rabbit secondary antibody (Promega, Madison, WI).

For IP, Protein A-Sepharose was used to preclear cell lysates (200–500 μg) for 1 hour at 4°C before removing and incubating cell supernatants with appropriate antibody (e.g. Lnk) for 2–16 hours at 4°C (Millipore). After incubating for 30–60 minutes, antigen-antibody complexes were recovered with rabbit anti-mouse immunoglobulin and protein A-Sepharose or protein A-Sepharose alone. Immune complexes were washed 3–5 times with lysis buffer,

and proteins were eluted into SDS-PAGE sample buffer (3% SDS, 60mM Tris, pH 6.9, 2 mM EDTA, 4% glycerol) by heating samples to 100°C for 5 minutes.

Under reducing conditions, immunoprecipitated samples (total cell lysates, 25–30 μg) were analyzed by 10% SDS-PAGE. Proteins were transferred to nitrocellulose via electrophoresis and Western blotted as described in the ECL system (Amersham, Pittsburgh, PA). For blot reprobing, nitrocellulose membranes were stripped of antibodies in a solution containing glycine (0.1 M; pH2.8) at 55°C for 30 minutes.

### STATISTICS

All data are presented as the Mean ± 1 SD unless otherwise stated. Experiments were performed at least three times in duplicate or triplicate. *In vivo* study sample sizes are presented in the corresponding figure legends, and Student's *t*-tests were performed when only two groups were compared. As male and female mouse bones exhibit virtually identical properties, for ease of reporting, and to increase sample size, data from male and female mice were combined for all *in vivo* data analysis. One-way Analysis of Variance (ANOVA) with least significant difference (LSD) was used to make multiple group comparisons.

## RESULTS

### Anthropometrics, Cortical Bone, Biomechanical and Biomaterial Properties

Body weight of $Lnk^{-/-}$ and WT C57BL/6 mice were similar for 20 week-old mice. Similarly, no significant differences were detected between $Lnk^{-/-}$ and WT mice for femoral length, mid-shaft width (medial to lateral), or mid-shaft height (ventral to dorsal) (Table 1) with respect to femoral geometry. Consistent with the mid-shaft width and height the cross-sectional area (CSA, Table 1), polar moment of inertia (Table 2) revealed a non-significant increase with Lnk deficiency.

However, the bone area (BA) was found to be significantly higher in WT femurs compared to $Lnk^{-/-}$ femurs (10% increase, $p<0.01$). $Lnk^{-/-}$ mice displayed a significant 78% increase in periosteal bone formation rate ($p<0.01$), but no difference in endocortical bone formation rate was observed.

With regard to biomechanical properties, $Lnk^{-/-}$ femurs were significantly less strong (12% reduction, $p<0.001$), less stiff (19% reduction, $p<0.001$), and failed at lower loads (15% reduction, $p<0.001$) than their WT mice. The modulus was also significantly lower (27% reduction, $p<0.001$) in $Lnk^{-/-}$ femurs compared to that observed in controls.

### TRABECULAR BONE PHENOTYPE OF 20-WEEK-OLD $LNK^{-/-}$ Mice

With respect to trabecular bone analyses, static histomorphometry and μCT data were obtained and are reported in Table 3 and Figure 1. Bone volume/tissue volume (BV/TV) was significantly elevated 2.5-fold in $Lnk^{-/-}$ mice compared to WT controls ($p=0.005$) by static histomorphometry, and 2.1-fold ($p<0.001$) by μCT. Structural indices of bone analysis revealed a significant increase in trabecular number (Tb.N, 2.3-fold increase, $p<0.001$) with concomitant decrease in trabecular separation (Tb.Sp, 1.4-fold decrease, $p<0.001$) in $Lnk^{-/-}$ femurs compared to WT controls. No differences were detected in trabecular thickness

(Tb.Th). There was a significant, 11% reduction ($p<0.001$) detected in the structural model index (SMI) in $Lnk^{-/-}$ femurs compared to WT femurs.

Further examination between WT and $Lnk^{-/-}$ femurs with respect to static bone histomorphometry parameters illustrated at 5 months of age there were no significant differences in the number of OB/tissue area (N.Ob/TAR) between $Lnk^{-/-}$ and WT femurs. However, there was a significant 1.7-fold increase in the number of OCs/tissue area (N.Oc/TAR, $p=0.001$) in $Lnk^{-/-}$ femurs compared to that observed in WT mice. Dynamic bone histomorphometric analyses revealed a significant 1.3-fold decrease ($p<0.05$) in bone formation rate/tissue volume (BRF/TV) and a 1.2-fold decrease ($p<0.05$) in mineral apposition rate (MAR).

## LNK IS EXPRESSED IN OSTEOBLAST LINEAGE CELLS

Since global deficiency of Lnk resulted in a high bone mass phenotype by 5 months of age with changes in both bone formation and resorption parameters *in vivo*, we investigated possible cellular mechanisms leading to this phenotype. First, we examined cells of the OB lineage. As shown in Figure 2A, expression of Lnk was observed in MKs (positive control) and in WT OB, but not in $Lnk^{-/-}$ (negative control).

## LNK EXPRESSION DOES NOT IMPACT OSTEOBLAST PROLIFERATION

To begin to understand the role of Lnk expression in OB function, we next sought to determine whether Lnk expression affected OB number or cell cycle regulation. To accomplish this, equal numbers of WT and $Lnk^{-/-}$ OB were seeded and assessed on days 1, 3, 5, and 7 for the total number of viable OB (trypan blue exclusion) produced in culture as well as their cell cycle status (Fig 2B, C). No differences in OB number or cell cycle were observed. Of interest, we also cultured OB in the presence or absence of TPO (Peprotech, Rocky Hill, NJ). Supplementation with 100 ng/ml of TPO did not have an effect on total number of OB progeny or their cell cycle status. Finally, we also assessed apoptosis by examining the expression of Annexin V. In all cases, less than 2% of the OB were Annexin V positive, suggesting that apoptosis was not altered based on genotype or TPO supplementation.

## LNK EXPRESSION DOES NOT AFFECT OB DIFFERENTIATION IN VITRO

To understand the effects of Lnk expression and signaling on OB differentiation, we examined the following four groups of cells: WT OB, WT OB + TPO, $Lnk^{-/-}$ OB, $Lnk^{-/-}$ OB + TPO. Cells were cultured under osteogenic conditions as detailed above. As shown in Figure 3A and B, we assessed alkaline phosphatase activity and measured bound calcium as a functional measure of mineralization after 10 or 14 days, respectively. No significant differences were detected between WT and $Lnk^{-/-}$ OB for mineralization (Figure 3A), but $Lnk^{-/-}$ OB alkaline phosphatase activity was markedly reduced (Figure 3B). Furthermore, the addition of 100 ng/ml of TPO did not have a notable effect on WT or $Lnk^{-/-}$ OB alkaline phosphatase activity or mineralization.

### THE EFFECTS OF LNK EXPRESSION ON OC

Next, we examined whether cells of the OC lineage express Lnk. In Figure 4A, using Western blot analysis we show Lnk is expressed in BMM (OC progenitors), RAW 264.7 cells (OC progenitor cell line), and MK (positive control). We then examined the ability of WT and Lnk BMM to differentiate into OC. Figure 4B shows OC number when C57BL/6 and $Lnk^{-/-}$ BMM were cultured with M-CSF (30 ng/ml) and RANKL (50 ng/ml) in the absence or presence of 100 ng/ml TPO. Only $TRAP^{+}$ multinucleated cells (>3 nuclei) were counted. TPO significantly enhanced OC number in cells generated from C57BL/6 and $Lnk^{-/-}$ mice. Significantly ($p<0.05$) more OC were generated from $Lnk^{-/-}$ mice compared to WT mice. OC cell counts were normalized to 100 in the WT controls (0 ng/ml TPO) for ease of comparison.

## DISCUSSION

Several mouse models with megakaryocytosis have been associated with the development of a high bone mass phenotype resulting from MK-mediated increase in OB proliferation and bone formation. We previously showed that *in vitro* MK enhance OB proliferation 3–6 fold by a direct cell-to-cell contact mechanism [Kacena et al., 2004]. Prior *in vivo* studies support our *in vitro* evidence that MK induce an OB proliferative net increase in bone formation, as mice overexpressing the MK growth factor TPO, experience a marked 4-fold increase in absolute MK number versus WT controls and develop a myelofibrotic syndrome with osteosclerosis by nine months of age [Frey et al., 1998; Villeval et al., 1997; Yan et al., 1995; Yan et al., 1996]. Considering this trend and the inhibitory regulation of TPO/c-mpl signaling by Lnk regulation of TPO, the main MK growth factor, we hypothesized that $Lnk^{-/-}$ mice would also have a high bone mass phenotype. Here we examine a similar mouse model involving dysregulation of TPO signaling. However, instead of up-regulating TPO expression, we instead removed Lnk, a negative regulator of TPO signaling, which allows for increased communication between TPO and its receptor, c-mpl.

In this study we examined the bone mass phenotype of $Lnk^{-/-}$ mice. Like the TPO overexpression model, $Lnk^{-/-}$ mice have an expected increase in MK number, and taken collectively the above data predict that the increased TPO-c-mpl signaling would also lead to a similar high bone mass phenotype (likely owing to increased MK stimulating increases on OB and bone formation). As predicted, $Lnk^{-/-}$ mice developed high bone mass compared to WT controls. Specifically, at 5 months of age $Lnk^{-/-}$ femurs had significant elevated trabecular BV/TV and Tb.N with a concomitant decrease in Tb.Sp. However, histomorphometric analysis did not show the predicted increase in N.Ob/T.Ar or BFR/TV. Indeed, no differences in N.Ob/T.Ar were observed and BFR/TV was actually significantly reduced in $Lnk^{-/-}$ femurs. We posit these seemingly contradictory findings are a result of the timing of these studies. We suggest that MK stimulated OB proliferation and bone deposition at an earlier time, which was not captured here, but resulted in the increase in BV/TV (a high turnover state like previously reported in other mouse strains with megakaryocytosis and high bone mass) [Frey et al., 1998; Kacena et al., 2004; Villeval et al., 1997; Yan et al., 1995; Yan et al., 1996]. The numbers of active OB then likely normalized with time. Of note, when we examined OB lineage cells generated from $Lnk^{-/-}$ and WT

mice, we found that while OB express Lnk, no differences in proliferation or mineralization were observed, although reduced alkaline phosphatase activity was observed in OB generated from $Lnk^{-/-}$ mice. That said, stimulation with TPO did not impact any of these in vitro findings. This suggests that Lnk itself may impact OB function (alkaline phosphatase activity) but at least based on our assays reported here, these parameters were not altered by stimulation of cells with TPO (Figs 2 and 3).

In addition to examining the impact of Lnk expression on OB lineage cells, we also examined the impact of Lnk expression on OC lineage cells. We found that OC progenitors express Lnk and that generation of mature OC from $Lnk^{-/-}$ mice resulted in a significant upregulation in mature OC number in vitro (Fig 4) and in vivo as was documented by the significant upregulation in N.Oc/T.Ar observed in $Lnk^{-/-}$ mice (Table 3). Further, we demonstrated that stimulation of OC progenitors with TPO increased mature OC number in cultures generated from both WT and $Lnk^{-/-}$ mice (the former confirms our previous findings, [Bethel et al., 2015]). $Lnk^{-/-}$ OC progenitors are more responsive to TPO presumably because removal of Lnk improves TPO signaling.

That said, it is possible that although OC number increases, bone resorbing activity in $Lnk^{-/-}$ OC may be altered.

It is important to realize that our group and others have previously demonstrated that MK can inhibit OC formation *in vitro* [Beeton et al., 2006; Kacena et al., 2006b; Wakikawa et al., 1997]. Indirectly, MK have been implicated to inhibit osteoclastogenesis by increasing OB expression of osteoprotegerin (OPG), a known inhibitor of OC formation [Bord et al., 2005]. In addition, MK have been implicated as secreting a, yet to be identified, factor(s) which can significantly inhibit OC development *in vitro* [Kacena et al., 2006a]. Interestingly, these studies and recently published studies from our laboratory demonstrate TPO and MK opposing roles in the regulation of OC formation [Bethel et al., 2015].

Although the interaction between BM cells such as MK and OB lineage cells occurs in the BM cavity where trabecular bone parameters were measured, we would be remiss if we did not examine the cortical bone phenotype observed in these mice. To this end, cortical histomorphometric and μCT parameters as well as biomechanical properties were assessed in $Lnk^{-/-}$ and WT mice. WT femurs proved stronger, stiffer, and had a higher ultimate failure than did $Lnk^{-/-}$ femurs. The observed increases in WT biomechanical properties are likely owing to the increase in cortical BA observed in WT mice with the same overall outer geometry (e.g. no significant differences in gross femur width or height and no differences in CSA).

Further, we would be remiss not to mention that there are other cell lineages directly affected by Lnk deficiency with noted effects on skeletal homeostasis. Indeed, Takaki et al showed $Lnk^{-/-}$ mice to have defective B lymphocyte production, with increased numbers of B cells in the BM cavity and spleen [Takaki et al., 2000]. Importantly, there exist at least 2 mouse models with defects in B-lymphocyte development, and conflicting effects on skeletal homeostasis. In fact, absence of Pax5, the gene coding for B-lymphocyte transcription factor, leads to arrested B-cell development, an increase in OC progenitor number, and

develop early onset osteopenia [Horowitz et al., 2004]. Conversely, mice deficient in EBF-1, another B-cell transcription factor, have increased OB and increased bone formation parameters [Horowitz and Lorenzo, 2007]. Thus B-lymphocytes are another cell lineage directly affected in $Lnk^{-/-}$ mice which may contribute to changes in bone homeostasis for this model.

The significance of these findings lends to recognition of the difficulties of interpreting results of cell lineages studied *in vitro*, isolated from their natural tissue environment. Figure 5 is a schematic representation illustrating the complexity of the cell-cell interactions as described in our present findings and previously published data [Meijome et al., 2015]. The BM cavity contains MK, OB, OC, and TPO. Bone phenotype is a result of a complex interplay between all elements. In prior mouse models, the proliferative effect of MK on OB was the presumed dominant interaction. In $Lnk^{-/-}$ mice, however, it appears that this direct and indirect effect of TPO on OC formation is also of critical importance.

By continuing to dissect the interaction between hematopoietic and bone cell lineages, the mechanisms regulating skeletal homeostasis are clarified. A better understanding of skeletal pathology and diseases of dysregulated bone turnover will pave the way for future therapeutic intervention.

## Acknowledgments

**Contract grant sponsor:** NIH

**Contract grant number:** DK090948, UL1TR001108, AR060863, AR060332, DK007519

The authors have no conflicts of interest to declare.

This work was supported by the Department of Orthopaedic Surgery, Indiana University School of Medicine (MAK), the Center of Excellence in Molecular Hematology funded in part by NIH/NIDDK DK090948, the Indiana - Clinical and Translational Sciences Institute funded in part by NIH grants UL1TR001108 (MAK, AB), NIH/NIAMS grants AR060863 (MAK) and AR060332 (MAK, AB), and NIH T32 DK007519 (DJO). We would like to thank Dr. Tony Pawson for providing the $Lnk^{-/-}$ mice.

## References

Beeton CA, Bord S, Ireland D, Compston JE. Osteoclast formation and bone resorption are inhibited by megakaryocytes. Bone. 2006; 39:985–90. [PubMed: 16870519]

Bethel M, Barnes CL, Taylor AF, Cheng YH, Chitteti BR, Horowitz MC, Bruzzaniti A, Srour EF, Kacena MA. A novel role for thrombopoietin in regulating osteoclast development in humans and mice. J Cell Physiol. 2015; 230:2142–51. [PubMed: 25656774]

Bord S, Ireland DC, Moffatt P, Thomas GP, Compston JE. Characterization of osteocrin expression in human bone. J Histochem Cytochem. 2005; 53:1181–7. [PubMed: 15923362]

Breton-Gorius J, Clezardin P, Guichard J, Debili N, Malaval L, Vainchenker W, Cramer EM, Delmas PD. Localization of platelet osteonectin at the internal face of the alpha-granule membranes in platelets and megakaryocytes. Blood. 1992; 79:936–41. [PubMed: 1737102]

Chagraoui H, Tulliez M, Smayra T, Komura E, Giraudier S, Yun T, Lassau N, Vainchenker W, Wendling F. Stimulation of osteoprotegerin production is responsible for osteosclerosis in mice overexpressing TPO. Blood. 2003; 101:2983–9. [PubMed: 12506018]

Cheng YH, Hooker RA, Nguyen K, Gerard-O'Riley R, Waning DL, Chitteti BR, Meijome TE, Chua HL, Plett AP, Orschell CM, Srour EF, Mayo LD, Pavalko FM, Bruzzaniti A, Kacena MA. Pyk2 regulates megakaryocyte-induced increases in osteoblast number and bone formation. J Bone Miner Res. 2013; 28:1434–45. [PubMed: 23362087]

Cheng YH, Streicher DA, Waning DL, Chitteti BR, Gerard-O'Riley R, Horowitz MC, Bidwell JP, Pavalko FM, Srour EF, Mayo LD, Kacena MA. Signaling pathways involved in megakaryocyte-mediated proliferation of osteoblast lineage cells. J Cell Physiol. 2015; 230:578–86. [PubMed: 25160801]

Chenu C, Delmas PD. Platelets contribute to circulating levels of bone sialoprotein in human. J Bone Miner Res. 1992; 7:47–54. [PubMed: 1549958]

Chitteti BR, Cheng YH, Streicher DA, Rodriguez-Rodriguez S, Carlesso N, Srour EF, Kacena MA. Osteoblast lineage cells expressing high levels of Runx2 enhance hematopoietic progenitor cell proliferation and function. J Cell Biochem. 2010; 111:284–94. [PubMed: 20506198]

Ciovacco WA, Cheng YH, Horowitz MC, Kacena MA. Immature and mature megakaryocytes enhance osteoblast proliferation and inhibit osteoclast formation. J Cell Biochem. 2010; 109:774–81. [PubMed: 20052670]

Ciovacco WA, Goldberg CG, Taylor AF, Lemieux JM, Horowitz MC, Donahue HJ, Kacena MA. The role of gap junctions in megakaryocyte-mediated osteoblast proliferation and differentiation. Bone. 2009; 44:80–6. [PubMed: 18848655]

Drachman JG, Sabath DF, Fox NE, Kaushansky K. Thrombopoietin signal transduction in purified murine megakaryocytes. Blood. 1997; 89:483–92. [PubMed: 9002950]

Eleniste PP, Patel V, Posritong S, Zero O, Largura H, Cheng YH, Himes ER, Hamilton M, Baughman J, Kacena MA, Bruzzaniti A. Pyk2 and Megakaryocytes Regulate Osteoblast Differentiation and Migration Via Distinct and Overlapping Mechanisms. J Cell Biochem. 2016; 117:1396–406. [PubMed: 26552846]

Feher A, Koivunemi A, Koivunemi M, Fuchs RK, Burr DB, Phipps RJ, Reinwald S, Allen MR. Bisphosphonates do not inhibit periosteal bone formation in estrogen deficient animals and allow enhanced bone modeling in response to mechanical loading. Bone. 2010; 46:203–7. [PubMed: 19857619]

Frank JD, Balena R, Masarachia P, Seedor JG, Cartwright ME. The effects of three different demineralization agents on osteopontin localization in adult rat bone using immunohistochemistry. Histochemistry. 1993; 99:295–301. [PubMed: 8500993]

Frey BM, Rafii S, Teterson M, Eaton D, Crystal RG, Moore MA. Adenovector-mediated expression of human thrombopoietin cDNA in immune-compromised mice: insights into the pathophysiology of osteomyelofibrosis. J Immunol. 1998; 160:691–9. [PubMed: 9551904]

Horowitz MC, Fields A, DeMeo D, Qian HY, Bothwell AL, Trepman E. Expression and regulation of Ly-6 differentiation antigens by murine osteoblasts. Endocrinology. 1994; 135:1032–43. [PubMed: 7520861]

Horowitz MC, Lorenzo JA. Immunologic regulation of bone development. Adv Exp Med Biol. 2007; 602:47–56. [PubMed: 17966387]

Horowitz MC, Xi Y, Pflugh DL, Hesslein DG, Schatz DG, Lorenzo JA, Bothwell AL. Pax5-deficient mice exhibit early onset osteopenia with increased osteoclast progenitors. J Immunol. 2004; 173:6583–91. [PubMed: 15557148]

Huang X, Li Y, Tanaka K, Moore KG, Hayashi JI. Cloning and characterization of Lnk, a signal transduction protein that links T-cell receptor activation signal to phospholipase C gamma 1, Grb2, and phosphatidylinositol 3-kinase. Proc Natl Acad Sci U S A. 1995; 92:11618–22. [PubMed: 8524815]

Hughes, FJ., Aubin, JE. Culture of cells of the osteoblast lineage. Arnett, TR., Henderson, B., editors. London: Chapman-Hall Ltd; 1998. p. 37

Jilka RL, Cohn DV. Role of phosphodiesterase in the parathormone-stimulated adenosine 3′,5′-monophosphate response in bone cell populations enriched in osteoclasts and osteoblasts. Endocrinology. 1981; 109:743–7. [PubMed: 6167435]

Kacena MA, Eleniste PP, Cheng YH, Huang S, Shivanna M, Meijome TE, Mayo LD, Bruzzaniti A. Megakaryocytes regulate expression of Pyk2 isoforms and caspase-mediated cleavage of actin in osteoblasts. J Biol Chem. 2012; 287:17257–68. [PubMed: 22447931]

Kacena MA, Gundberg CM, Horowitz MC. A reciprocal regulatory interaction between megakaryocytes, bone cells, and hematopoietic stem cells. Bone. 2006a; 39:978–84. [PubMed: 16860008]

Kacena MA, Gundberg CM, Nelson T, Horowitz MC. Loss of the transcription factor p45 NF-E2 results in a developmental arrest of megakaryocyte differentiation and the onset of a high bone mass phenotype. Bone. 2005; 36:215–23. [PubMed: 15780947]

Kacena MA, Nelson T, Clough ME, Lee SK, Lorenzo JA, Gundberg CM, Horowitz MC. Megakaryocyte-mediated inhibition of osteoclast development. Bone. 2006b; 39:991–9. [PubMed: 16782418]

Kacena MA, Shivdasani RA, Wilson K, Xi Y, Troiano N, Nazarian A, Gundberg CM, Bouxsein ML, Lorenzo JA, Horowitz MC. Megakaryocyte-osteoblast interaction revealed in mice deficient in transcription factors GATA-1 and NF-E2. J Bone Miner Res. 2004; 19:652–60. [PubMed: 15005853]

Kelm RJ Jr, Hair GA, Mann KG, Grant BW. Characterization of human osteoblast and megakaryocyte-derived osteonectin (SPARC). Blood. 1992; 80:3112–9. [PubMed: 1467517]

Meijome TE, Baughman JT, Hooker RA, Cheng YH, Ciovacco WA, Balamohan SM, Srinivasan TL, Chitteti BR, Eleniste PP, Horowitz MC, Srour EF, Bruzzaniti A, Fuchs RK, Kacena MA. C-Mpl Is Expressed on Osteoblasts and Osteoclasts and Is Important in Regulating Skeletal Homeostasis. J Cell Biochem. 2015

Pearse RN, Sordillo EM, Yaccoby S, Wong BR, Liau DF, Colman N, Michaeli J, Epstein J, Choi Y. Multiple myeloma disrupts the TRANCE/ osteoprotegerin cytokine axis to trigger bone destruction and promote tumor progression. Proc Natl Acad Sci U S A. 2001; 98:11581–6. [PubMed: 11562486]

Simmons DJ, Kent GN, Jilka RL, Scott DM, Fallon M, Cohn DV. Formation of bone by isolated, cultured osteoblasts in millipore diffusion chambers. Calcif Tissue Int. 1982; 34:291–4. [PubMed: 6809292]

Sipe JB, Zhang J, Waits C, Skikne B, Garimella R, Anderson HC. Localization of bone morphogenetic proteins (BMPs)-2, -4, and -6 within megakaryocytes and platelets. Bone. 2004; 35:1316–22. [PubMed: 15589212]

Srour EF, Brandt JE, Leemhuis T, Ballas CB, Hoffman R. Relationship between cytokine-dependent cell cycle progression and MHC class II antigen expression by human CD34+ HLA-DR− bone marrow cells. J Immunol. 1992; 148:815–20. [PubMed: 1370518]

Stanford CM, Jacobson PA, Eanes ED, Lembke LA, Midura RJ. Rapidly forming apatitic mineral in an osteoblastic cell line (UMR 106-01 BSP). J Biol Chem. 1995; 270:9420–8. [PubMed: 7721867]

Suva LJ, Hartman E, Dilley JD, Russell S, Akel NS, Skinner RA, Hogue WR, Budde U, Varughese KI, Kanaji T, Ware J. Platelet dysfunction and a high bone mass phenotype in a murine model of platelet-type von Willebrand disease. Am J Pathol. 2008; 172:430–9. [PubMed: 18187573]

Takaki S, Sauer K, Iritani BM, Chien S, Ebihara Y, Tsuji K, Takatsu K, Perlmutter RM. Control of B cell production by the adaptor protein lnk. Definition Of a conserved family of signal-modulating proteins. Immunity. 2000; 13:599–609. [PubMed: 11114373]

Takaki S, Watts JD, Forbush KA, Nguyen NT, Hayashi J, Alberola-Ila J, Aebersold R, Perlmutter RM. Characterization of Lnk. An adaptor protein expressed in lymphocytes. J Biol Chem. 1997; 272:14562–70. [PubMed: 9169414]

Thiede MA, Smock SL, Petersen DN, Grasser WA, Thompson DD, Nishimoto SK. Presence of messenger ribonucleic acid encoding osteocalcin, a marker of bone turnover, in bone marrow megakaryocytes and peripheral blood platelets. Endocrinology. 1994; 135:929–37. [PubMed: 8070388]

Tong W, Lodish HF. Lnk inhibits Tpo-mpl signaling and Tpo-mediated megakaryocytopoiesis. J Exp Med. 2004; 200:569–80. [PubMed: 15337790]

Velazquez L, Cheng AM, Fleming HE, Furlonger C, Vesely S, Bernstein A, Paige CJ, Pawson T. Cytokine signaling and hematopoietic homeostasis are disrupted in Lnk-deficient mice. J Exp Med. 2002; 195:1599–611. [PubMed: 12070287]

Villeval JL, Cohen-Solal K, Tulliez M, Giraudier S, Guichard J, Burstein SA, Cramer EM, Vainchenker W, Wendling F. High thrombopoietin production by hematopoietic cells induces a fatal myeloproliferative syndrome in mice. Blood. 1997; 90:4369–83. [PubMed: 9373248]

Wakikawa T, Shioi A, Hino M, Inaba M, Nishizawa Y, Tatsumi N, Morii H, Otani S. Thrombopoietin inhibits in vitro osteoclastogenesis from murine bone marrow cells. Endocrinology. 1997; 138:4160–6. [PubMed: 9322925]

Warden SJ, Nelson IR, Fuchs RK, Bliziotes MM, Turner CH. Serotonin (5-hydroxytryptamine) transporter inhibition causes bone loss in adult mice independently of estrogen deficiency. Menopause. 2008; 15:1176–83. [PubMed: 18725867]

Weatherholt AM, Fuchs RK, Warden SJ. Cortical and trabecular bone adaptation to incremental load magnitudes using the mouse tibial axial compression loading model. Bone. 2013; 52:372–9. [PubMed: 23111313]

Wong GL, Cohn DV. Target cells in bone for parathormone and calcitonin are different: enrichment for each cell type by sequential digestion of mouse calvaria and selective adhesion to polymeric surfaces. Proc Natl Acad Sci U S A. 1975; 72:3167–71. [PubMed: 171656]

Yan XQ, Lacey D, Fletcher F, Hartley C, McElroy P, Sun Y, Xia M, Mu S, Saris C, Hill D, Hawley RG, McNiece IK. Chronic exposure to retroviral vector encoded MGDF (mpl-ligand) induces lineage-specific growth and differentiation of megakaryocytes in mice. Blood. 1995; 86:4025–33. [PubMed: 7492757]

Yan XQ, Lacey D, Hill D, Chen Y, Fletcher F, Hawley RG, McNiece IK. A model of myelofibrosis and osteosclerosis in mice induced by overexpressing thrombopoietin (mpl ligand): reversal of disease by bone marrow transplantation. Blood. 1996; 88:402–9. [PubMed: 8695786]

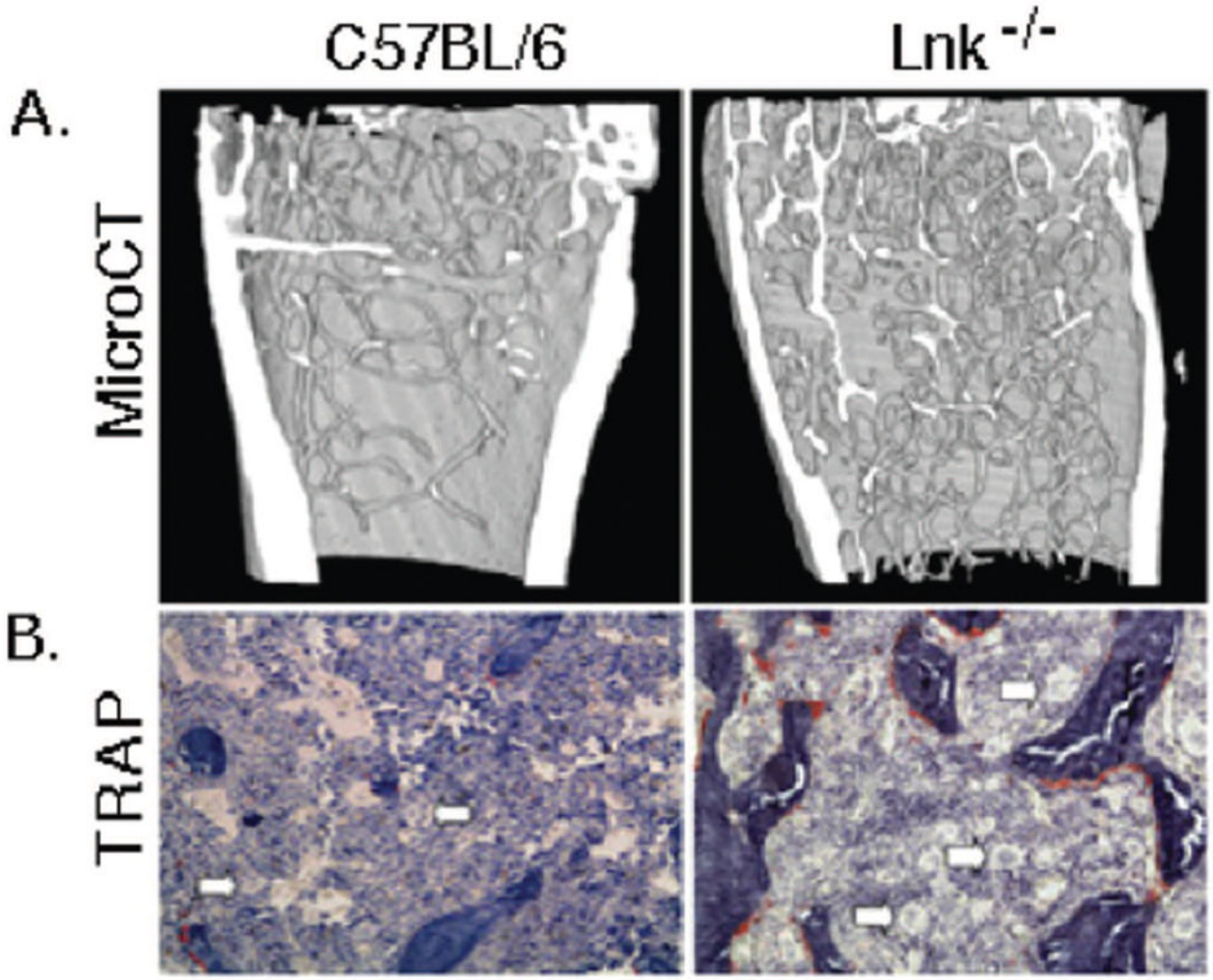


**Figure 1.**

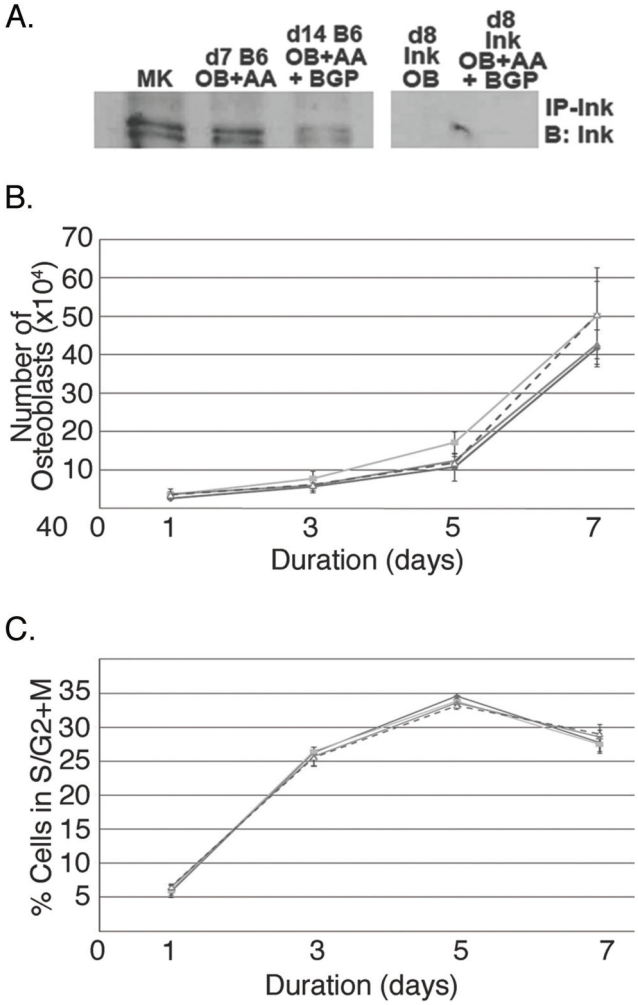


**Figure 2.**

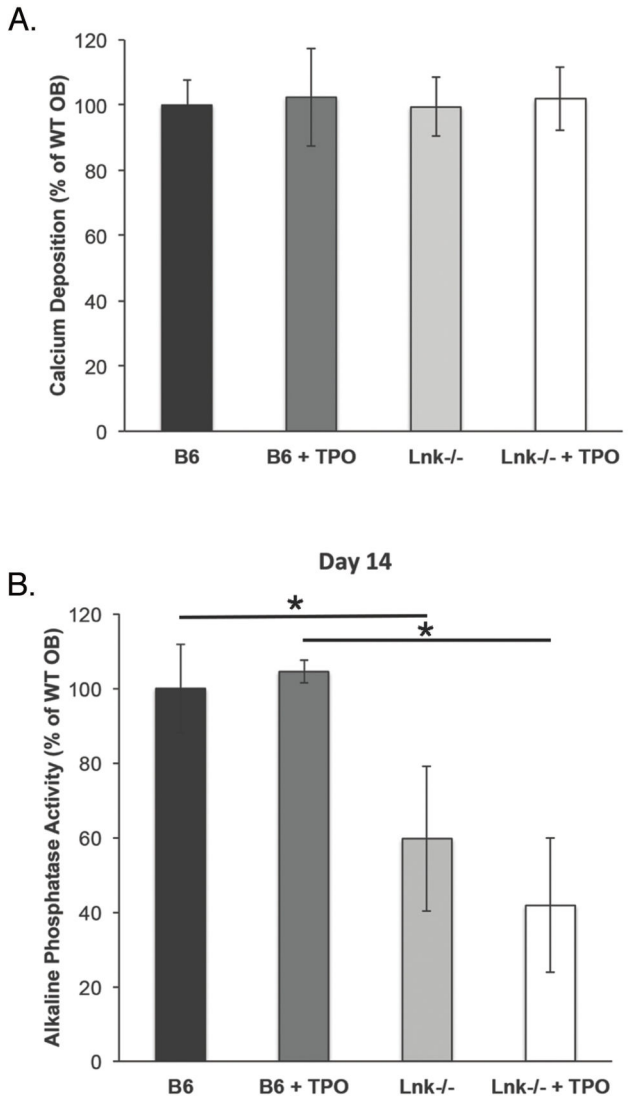


**Figure 3.**

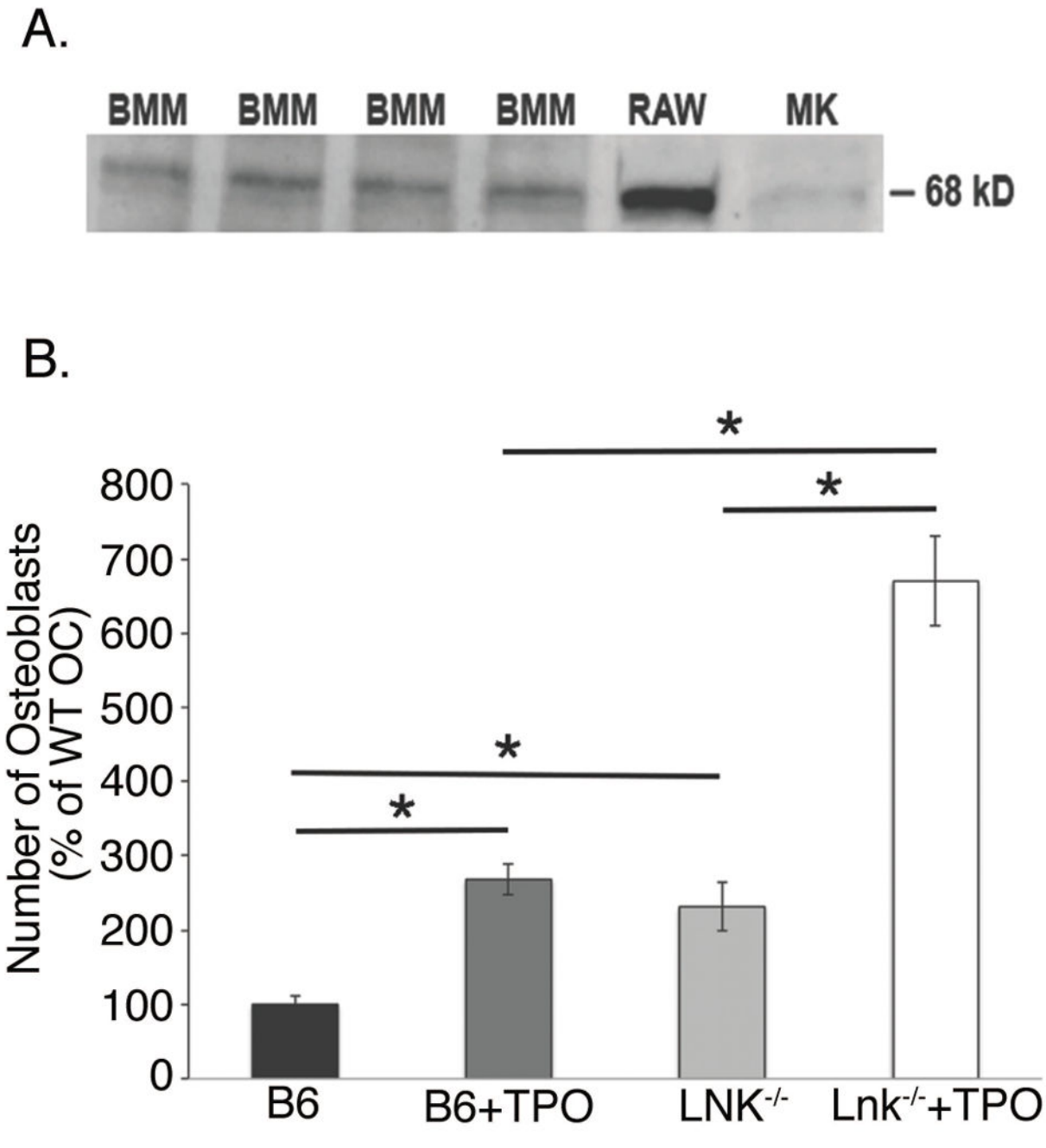


**Figure 4.**

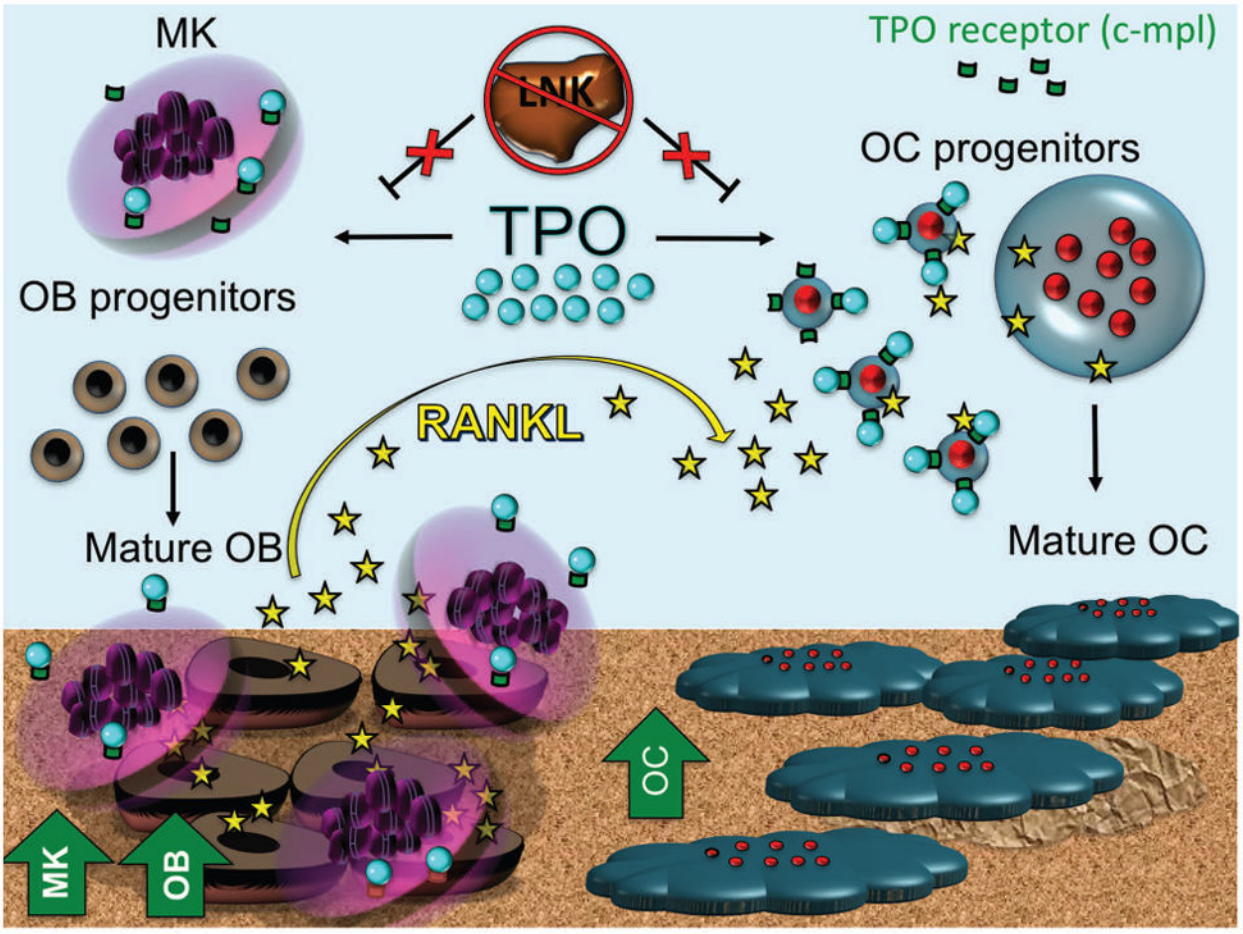


**Figure 5.**

**Table 1**

Anthropometrics and cortical bone histomorphometry properties, 20 week-old Lnk$^{-/-}$ and WT mice

| | Anthropometrics | | | | Cortical Bone Histomorphometry | | | | |
|---|---|---|---|---|---|---|---|---|---|
| **Mice** | **n** | **Length (mm)** | **Width (mm)** | **Height (mm)** | **n** | **CSA (μm$^2$)** | **BA (μm$^2$)** | **Periosteal BFR (μm$^2$/μm$^3$/day)** | **Endocortical BFR (μm$^2$/μm$^3$/day)** |
| C57BL/6 (WT) | 37 | 15.3 ± 0.1 | 1.74 ± 0.03 | 1.29 ± 0.02 | 19 | 1.72 ± 0.04 | 0.86 ± 0.05 | 17 ± 4 | 53 ± 2 |
| Lnk$^{-/-}$ | 18 | 15.3 ± 0.1 | 1.81 ± 0.04 | 1.28 ± 0.02 | 17 | 1.88 ± 0.07 | 0.77 ± 0.02 * | 32 ± 2 * | 48 ± 2 |

Length, distal to proximal femur length; Width, medial to lateral femur width; Height, ventral to dorsal femur height; CSA, cross-sectional area; BA, bone area; Periosteal BFR, periosteal bone formation rate; Endocortical BFR, endocortical bone formation rate.

Results are presented as mean ± SEM;

* Indicates significant difference compared with WT ($p<0.05$)

**Table 2**

Biomechanical biomaterial properties, 20 week-old $Lnk^{-/-}$ and WT mice

| Biomechanical and Biomaterial properties | | | | | | |
|---|---|---|---|---|---|---|
| **Mice** | **n** | **Polar MOI ($mm^4$)** | **Modulus (MPa)** | **Load at Peak (N)** | **Stiffness (N/mm)** | **Ultimate Failure (MPa)** |
| C57BL/6 (WT) | 37 | 0.36 ± 0.01 | 42797 ± 1697 | 23.0 ± 0.4 | 123 ± 4 | 249 ± 6 |
| $Lnk^{-/-}$ | 18 | 0.40 ± 0.02 | 31291 ± 2901 * | 20.3 ± 0.6 * | 100 ± 5 * | 211 ± 9 * |

Polar MOI, polar moment of inertia.

Results are presented as mean ± SEM;

* Indicates significant difference compared with WT ($p<0.05$)

**Table 3**

Trabecular bone: μCT and static histomorphometric analysis of the distal femur of 20 week-old $Lnk^{-/-}$ and WT mice

| | | MicroCT | | | | | | Histology | | | | |
|---|---|---|---|---|---|---|---|---|---|---|---|---|
| **Mice** | **n** | **BV/TV (%)** | **SMI** | **Tb.Th (mm)** | **Tb.N (1/mm)** | **Tb.Sp (mm)** | **n** | **BV/TV (%)** | **N.Ob/ T.Ar** | **N.Oc/ T.Ar** | **BFR/TV ($\mu m^3/\mu m^2$/year)** | **MAR (μm/day)** |
| C57BL/6 (WT) | 38 | 3.6 ± 0.3 | 2.7 ± 0.1 | 0.053 ± 0.002 | 0.69 ± 0.05 | 0.34 ± 0.01 | 12 | 3.9 ± 0.8 | 59 ± 13 | 29 ± 4 | 346 ± 33 | 1.8 ± 0.1 |
| $Lnk^{-/-}$ | 18 | 7.7 ± 0.7 * | 2.4 ± 0.1 * | 0.048 ± 0.002 | 1.6 ± 0.1 * | 0.25 ± 0.01 * | 18 | 9.8 ± 1.1 * | 52 ± 13 | 48 ± 4 * | 264 ± 16 * | 1.5 ± 0.1 * |

BV/TV, bone volume/tissue volume; SMI, structure model index; Tb.Th, trabecular thickness; Tb.N, trabecular number; Tb.Sp, trabecular spacing; BV/TV, bone volume/tissue volume; N.Ob/T.Ar, number of osteoblasts/tissue area; N.Oc/T.Ar, number of osteoclasts/tissue area; BFR/TV, bone formation rate/tissue volume; MAR, mineral apposition rate.

Results are presented as mean ± SEM;

* Indicates significant difference compared to WT ($p<0.05$)